

Review

# Review on Test Benches Studying Sliding Electrical Contact and Synthesis of Experimental Results

Théo Kziazyk<sup>1</sup>, Eric Gavignet<sup>1,\*</sup>, Pierre-Henri Cornuault<sup>2</sup> , Philippe Baucour<sup>1</sup> and Didier Chamagne<sup>1</sup>

<sup>1</sup> Energy Department, FEMTO-ST Institute, Université Franche-Comte, CNRS, 90000 Belfort, France

<sup>2</sup> Applied Mechanics Department, FEMTO-ST Institute, Université Franche-Comte, CNRS, 25000 Besançon, France

\* Correspondence: eric.gavignet@femto-st.fr

**Abstract:** Sliding electrical contacts are commonly used with a slip ring to collect the current in moving system generators, alternators, or electrical motors. These contacts are also found in electrical transports without batteries, which are mostly supplied by means of a pantograph–catenary system. These systems are fraught with numerous issues. Among them, it is worth highlighting wear and heating, which lead to failures and pre-worn materials. Moreover, with the increase in speed and improvements in technologies and materials, new problems emerge. This is the case with the substitution of the classic copper strip with graphite or copper-impregnated graphite. Multiple works that studied sliding electrical contacts have been achieved recently, some by trying to create a model of the system based on experimental results, and others only based on experimental works and measurements. This paper aims to review articles from this last category by making a synthesis of different test benches used and then by opening a discussion based on different results highlighted by scholars. This discussion is divided into five points that constitute the system inputs. These are the environment, material, normal load, sliding speed, and current. Based on this discussion, a conclusion attempts to evaluate topics where results and trends are commonly established by authors and topics where there is a lack of work or some conflicts in the results or trends between different articles. For this last point, some perspectives are given for further experimental works.

**Keywords:** sliding electrical contact; contact material; electric wear; pantograph–catenary interaction; slip ring interaction



**Citation:** Kziazyk, T.; Gavignet, E.; Cornuault, P.-H.; Baucour, P.; Chamagne, D. Review on Test Benches Studying Sliding Electrical Contact and Synthesis of Experimental Results. *Energies* **2023**, *16*, 1294. <https://doi.org/10.3390/en16031294>

Academic Editor: Francesco Bottiglione

Received: 16 December 2022

Revised: 11 January 2023

Accepted: 17 January 2023

Published: 25 January 2023



**Copyright:** © 2023 by the authors. Licensee MDPI, Basel, Switzerland. This article is an open access article distributed under the terms and conditions of the Creative Commons Attribution (CC BY) license (<https://creativecommons.org/licenses/by/4.0/>).

## 1. Introduction

In railway, automotive, or generating systems, sliding electrical contacts (SECs) are widely studied in components such as generators, alternators, or electrical motors. These contacts are used to conduct electricity from a static/dynamic system to another dynamic system. For example, in a railway system, a pantograph slides against a copper wire to supply the motors (Figure 1a) while rotating slip rings against brushes to carry the current in automotive or generating systems (Figure 1b). Therefore, the reliability and the lifetime of these systems are important.

Studying systems with SEC remains difficult because of the great number of properties and effects that have to be taken into account. Figure 2 lists the parameters, inputs, and outputs of an ideal experimental bench. The physical properties and phenomena depend on inputs but are also interlinked. Thus, some of these properties and phenomena have an indirect impact on the wear and the power supply quality.

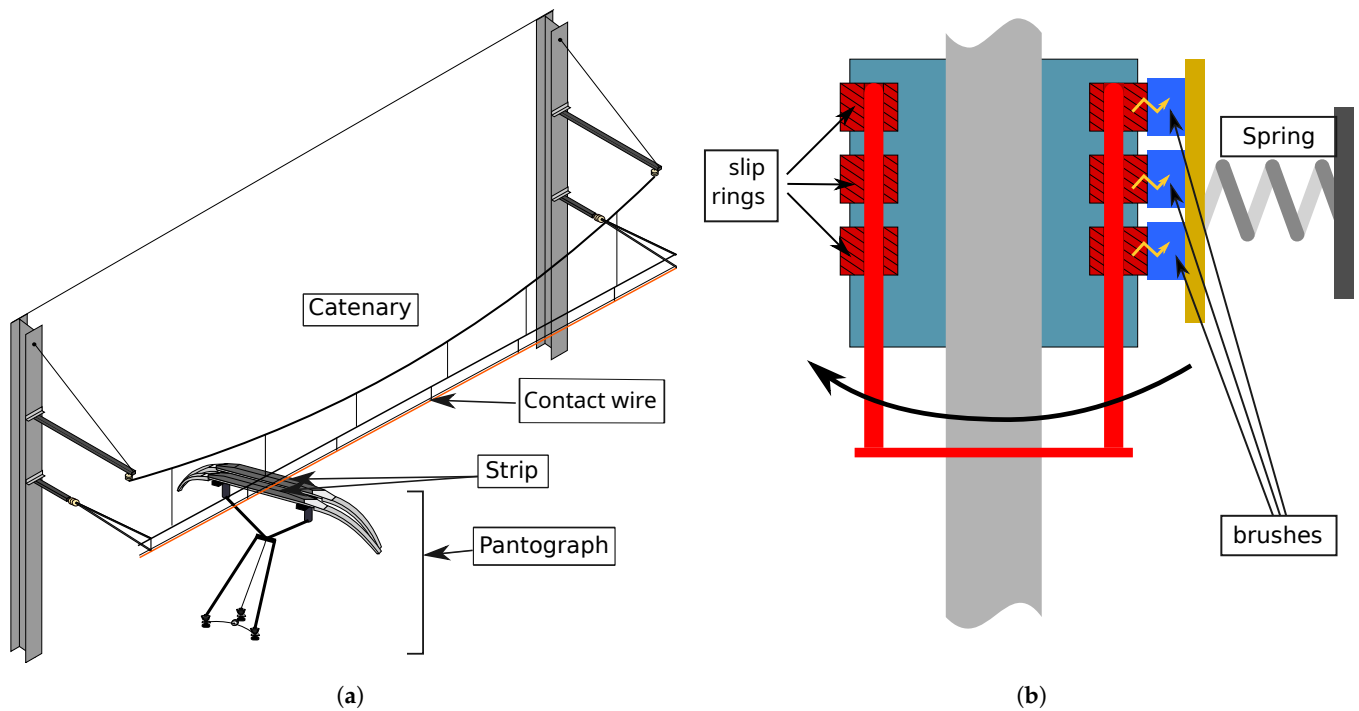


Figure 1. (a) Schematic of a pantograph–catenary system [1]. (b) Schematic of a slip ring.

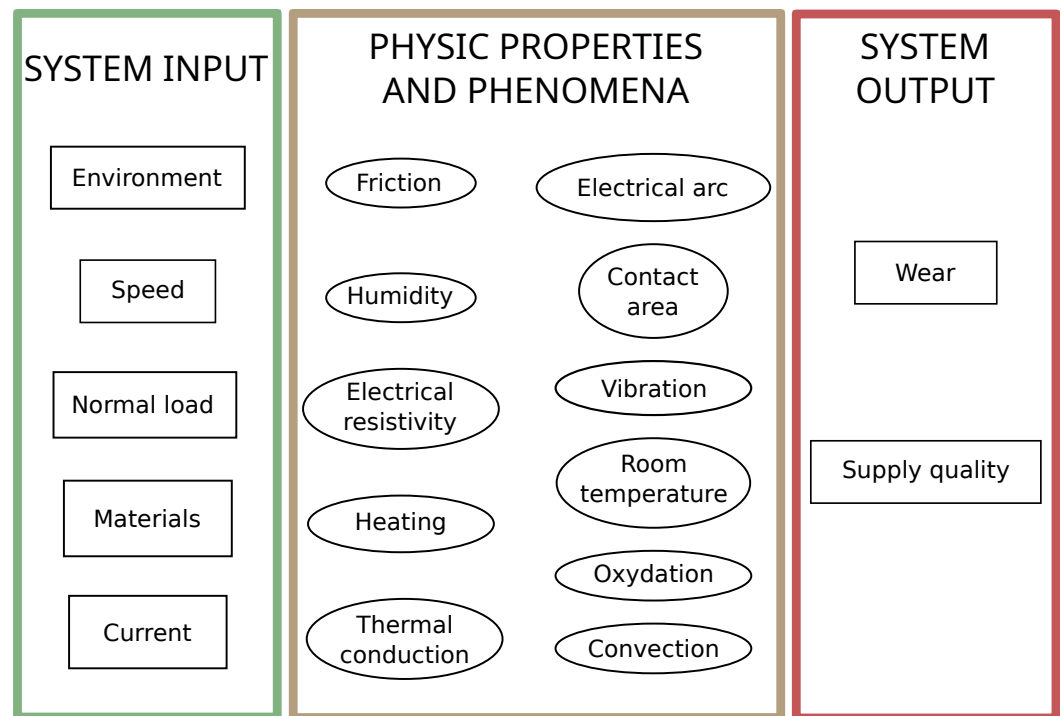


Figure 2. Description of the parameters of a sliding electrical contact.

The main inputs impacting a sliding electrical contact can be divided into five items: **The materials** relate to the wire contact/slip ring and the strip/brush. Wire contact and slip ring are mainly composed of copper whereas the materials composing the strips and brushes are more varied. They were first made of pure copper or steel but the system needed lubrication and the wire contact/slip ring as well as the strip/brushes suffered too much wear [2]. Graphite composite materials have been found to have an auto-lubricating property and a lower toughness than copper [3,4]. This partly resolved the issue of wire maintenance but it increased the electrical resistance of the contact, leading to an increase

in the heat produced into the contact [5]. Impregnating the graphite with copper partially solved this problem [6]. The materials used also define the geometry of the sliding contact and the apparent contact area. Moreover, roughness and asperity determine the real contact area.

**The current** relies on the energy needed by the system to fully work. It induces an increase in the heat released by the Joule effect. It also impacts the wear, friction coefficient, and arcing. Finally, the current impacts the third body formation [7]. This body will be detailed later and concerns the oxidation layer and the debris found between the two surfaces.

**The speed** increases vibrations and contact losses, leading to an increase in arc occurrences [8]. Speed also induces a cooling phenomenon due to air convection [9].

**The normal load** represents the normal force of the strip on the wire contact. It avoids contact loss between wire contact/slip ring and the strip/brushed, decreasing the arcing and increasing the real contact area [10]. However, the normal load also increases the friction coefficient and mechanical wear [11]. Furthermore, the normal load is known to fluctuate due to the geometry of the catenary [12].

**Environment** is the most difficult parameter to study and control. The environmental inputs include solar radiation, ambient temperature, frost, and humidity. For example, wind gust and turbulence can affect the contact reliability [13]. These parameters affect other physical properties and phenomena such as electrical resistivity, oxidation, or arcing [14,15].

These are the main inputs chosen by authors, but other properties can affect the contact quality. In the pantograph–catenary system, the irregularities of the catenary [16,17], its geometry [18], its height [19], and its wear [20,21] can have a noticeable effect on the contact behaviour. The properties of the pantograph such as the strip spacing [22] and the aerodynamics [23–25] can also be important to take into account.

Multiple models have been proposed to predict wear, such as a heuristic model [26,27] or FEM model [28]. Others tend to study the heat [1] or the aerodynamics of the pantograph [15]. Most of these models are tested based on experimental results. This review aims to describe different test benches made to study SEC and to discuss the main trends and results found by authors. Finally, a synthesis of the progress of numerous fields that composed SEC is given as a conclusion with some perspectives.

## 2. A Variety of Experimental Setups

Most of the test benches focused on the representativity of the sliding electrical contact found in industries or in railways transports. Representativeness can be assessed through materials, current or current density, contact area, normal load, or sliding speed. Some experimental setups aim to measure the temperature close to the contact. After experiments, wear measurements are also usually performed and friction track analyses are sometimes conducted using characterisation tools such as scanning electron microscopy (SEM) and energy dispersive spectroscopy (EDS). Table 1 lists the test benches that study the pantograph–catenary link whereas Table 2 presents the sliding contact in slip rings. Most of the experimental setup has a rotating part corresponding to the contact wire or the slip ring. In pressure with this part by means of strings, for example, one or two static parts simulate the strip or the brushes.

**Table 1.** List of test benches used to study pantograph–catenary contact \*. A(AC) stands for alternative current and A(DC) for direct current.

	Pin on Disc Tribotester [29]	Pin on Disc Tribotester [30,31]	Ring Block Test Bench [32,33]	Ring Block Test Bench [34–36]	Ring Block CCTB [1,27,37,38]
Speed	28 m.s <sup>-1</sup>	20 m.s <sup>-1</sup>	8.4 m.s <sup>-1</sup>	110 m.s <sup>-1</sup>	60 m.s <sup>-1</sup>
Normal load	70 N	70 N	80 N	10–300 N	60–110 N
Voltage Current *	300 A(AC) 50 Hz	100 A(AC) 125 Hz	200 A(AC)	400 A(AC) 100–3000 V; 700 A(DC) 15–180 V	1400 A(DC) 500 A(AC) 16 <sub>2/3</sub> Hz 350 A(AC) 50 Hz
Zigzag motion	None	None	Yes	Yes (0.3–3 Hz)	Yes
Arc detection	Photo diode	None	None	Hall effect current sensor	Contact voltage history
Temperature measurement	None	None	Infrared camera	Infrared camera	K-type Thermocouple
Wear measurement	None	Mass loss method	None	Volume loss distance	Instantaneous NWR mass difference
Friction measurement	None	Yes	None	Load cells	Load cells
Surface analysis	SEM, XPS 3D profiler	SEM, EDS density Hardness roughness	SEM, EDS	Digital camera SEM, EDS	None
Strip material	Pure carbon	Pure copper, Copper–graphite composites, Copper–graphite-coated,	Pure carbon	Pure carbon	Carbon, Carbon-impregnated Cu (20–30%)
Wire material	QCr0.5 chromium copper alloy	QCr0.5 chromium copper alloy	Copper–magnesium alloy	Copper–silver alloy	Pure copper
Particularity	Fluctuation of dynamic normal load	Study frictional behaviour, Study of current	Precise non-intrusive thermal measurement	Adjustable angle of strip	Full-scale experiments Use of different types of current

### 2.1. Experimental Study of Pantograph–Catenary Contacts

Three different types of test benches specializing in the study of the pantograph–catenary contact have been found in the modern literature.

#### 2.1.1. Current-Carrying Friction and Wear Tester Pin-on-Disc Tribometer

(In Table 1, see column 1 for the article by Zhang Y. [29] and column 2 for the article by Yang Z. [31]). A copper disc rotates against two pins made of the same materials. A current flows out of a pin through the disc sample and goes back from the other pin (see Figure 3). The current is alternative (125 Hz or 50 Hz) and can reach 300 A. Sliding speed is set to a maximum of 28 m.s<sup>-1</sup>.

The particularity in the first article is to use a photo-diode to evaluate the electrical arc intensity and a high-speed camera to record the arc discharge process with a 10,000 fps (frame per second) frame rate. The dynamic normal load, representative of the one found in a pantograph–catenary system, fluctuates periodically around 70 N, with precise amplitude and frequency. The impact of amplitude and frequency on the arcing rate is then studied [29].

The specific feature of the second work is to use three different materials as strips to study friction, wear, and current carrying performance. The wear rate is measured by the mass loss during a test while the measurement method of the friction coefficient is unclearly exposed. The current carrying performance is evaluated by measuring the current carrying efficiency and the current carrying stability. Efficiency is calculated by the average of the current measured by the current set. Stability corresponds to the fluctuation of the conduction current during service. It is calculated as follows:

$$\delta = \left(1 - \frac{\sigma}{\bar{I}_i}\right)100\% \quad (1)$$

where  $\delta$  is the current-carrying stability parameter [%],  $\sigma$  is the standard deviation for current [A],  $\bar{I}_i$  is the average value of the actual current during test [A].

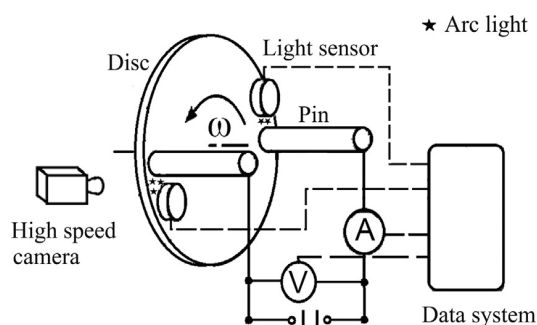


**Figure 3.** Configuration of the test bench from articles by Yang Z. et al. [29–31]. Copyright (2023), with permission from Elsevier.

**Table 2.** List of test benches used to study slip rings.

	Low-Speed Test Bench [39]	Tribological Test Device [40]	Test Bench of Brushes for Automotive Small Brush-Type DC Motor [41]	In Situ Experimental Test Bench of Metal Graphite Brush [42]	Friction Wear Tester for Cu-Ti <sub>3</sub> AlC <sub>2</sub> Brush [43]
<b>Speed</b>	0.02–0.5 m.s <sup>-1</sup>	10 m.s <sup>-1</sup>	15 m.s <sup>-1</sup>	14 m.s <sup>-1</sup>	15 m.s <sup>-1</sup>
<b>Normal load</b>	5–30 N	1.25–5 N	1.5–2.5 N	2.4 N	1.25–7.5 N.cm <sup>-2</sup>
<b>Current</b>	0–10 A	0–8 A(DC) 4.3 A.cm <sup>-2</sup>	5–20 A(DC)	1–5 A(DC) 3.4–17 A.cm <sup>-2</sup>	0–15 A.cm <sup>-2</sup>
<b>Arc detection</b>	None	None	None	None	None
<b>Temperature measurement</b>	K-type Thermocouple	K-type Thermocouple	T-type Thermocouple	T-type Thermocouple	None
<b>Wear measurement</b>	None	Measure with mass loss and distance	Measure with mass loss and distance	Measure with position difference before/after test	Calculated with mass loss
<b>Friction measurement</b>	3D piezoelectric sensor	None	Yes	None	Power loss method
<b>Mass loss measurement</b>	Before/after test	Before/after test	Before/after test	None	Before/after test
<b>Surface analysis</b>	OM, SEM EDS, 3D SP	3D optical microscope, SEM, white light interferometry, 3D SP	None	Digital camera	SEM, 3D surface profiler Raman Spectroscopy
<b>Brush material</b>	Electrographite DE9000	Hard carbon, electrographite, polymer-bonded, graphite	Copper–graphite brush	Metal graphite (40wt% Cu, 60wt% C)	Cu-30%Ti <sub>3</sub> AlC <sub>2</sub>
<b>Ring material</b>	Pure copper (99.9%)	Hard carbon electrographite polymer-bonded graphite	Copper	Copper (SE-Cu F25)	Cu-5%Ag
<b>Particularity</b>	Study at low speed	Use three different types of carbon, repeatability of results, contact surface given	Anode and cathode studied apart	Adjustable $T_{amb}$ Adjustable HR	Study of homemade Cu-Ti <sub>3</sub> AlC <sub>2</sub> composites

Three issues can be noticed in papers that emerged from these works. Firstly, it is not possible to know which sample is the cathode and the anode. Therefore, it is not specified in which direction the current flows at the contact of the sample studied. Furthermore, as there is no zig-zag motion, the wear rate measured during tests can be amplified due to overheating. Finally, as the system contains two contacts and not just one, the contact

losses occurrences are multiplied. This leads to a current-carrying efficiency and stability affected much quicker than in a system with one contact.

### 2.1.2. Ring Block-Type Test Machine

Test benches use one or two contact wires fixed at the outer edge of a rotating wheel (in Table 1, see column 3 for the first experimental setup [32,33] and column 4 for the second [34,35]). A strip is pushed so as to be in contact with these wires and is driven by a translation movement to represent the sweeping motion of a strip in real conditions. A current flows through the wire contact to the strip.

The first experimental bench (Figure 4a) helps to study contact temperature, using a non-intrusive infrared camera [32,33]. Its characteristics are listed in the third column of Table 1. The authors did not measure wear, they mainly studied the wear processes and the different wear morphology types using SEM, EDS, and observation.

The second experimental setup allows us to reach a sliding speed of  $110 \text{ m.s}^{-1}$ , but the maximum value used to study the pantograph–catenary contact is set to  $55 \text{ m.s}^{-1}$ . One peculiarity is to choose the angle between the strip and the contact wire, from  $0^\circ$  to  $4^\circ$ , and to observe its influence upon other parameters [34] (see Figure 4b). With the same test bench, Chen G.X. et al. [35] measure the arc discharge energy, using a Hall voltage sensor and a Hall current sensor. The cumulated arc discharge energy per unit of sliding distance, defined as the scaled accumulated energy by the authors, is then calculated with the formula:

$$E = \frac{\int UI dt}{d} \quad (2)$$

where  $E$  is the arc discharge energy [ $\text{J.km}^{-1}$ ],  $U$  stands for the arc voltage [V],  $I$  represents the electric current [A],  $d$  is the sliding distance [km], and  $t$  is the test time [s]. They also measure the temperature with an infrared camera and calculate the wear rate of the contact strip by dividing the volume loss  $V$  [ $\text{mm}^3$ ] by the covered distance  $d$ .

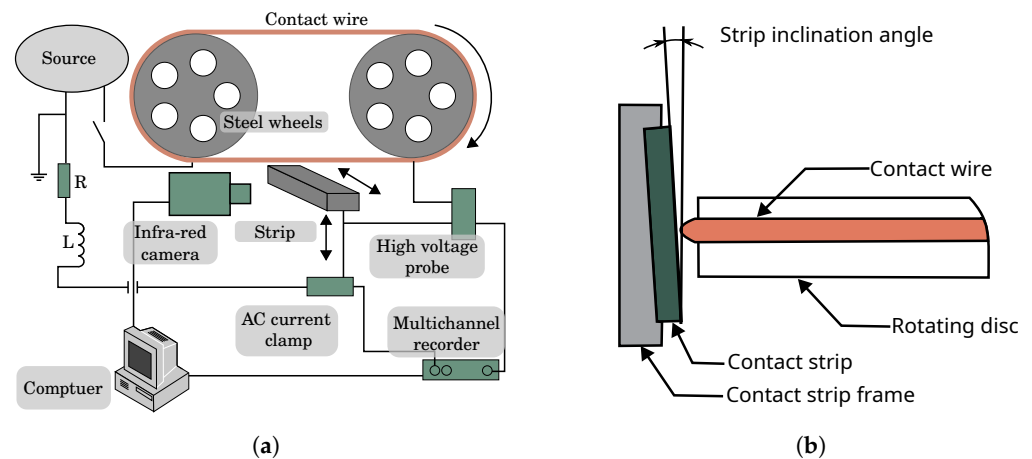


**Figure 4.** (a) Synoptic of the School of Electrical Engineering's test bench from an article by Wu G. et al. [33]. Copyright (2023), with permission from Elsevier. (b) Test bench synoptic of the Tribology Research Institute, Southwest Jiatong University, from an article by Chen G. et al. [34].

### 2.1.3. Full-Scale Experimental Ring Block

A ring block called CCTB (Current Collection Test Bench) has been built within the Mechanical Department of Politecnico di Milano [38] (in Table 1, see column 5). It is a full-scale pantograph–catenary system that reaches a sliding speed of  $60 \text{ m.s}^{-1}$ , with a sweeping movement between the contact wire and the strip. An airflow system is used to simulate the real convection of the airflow. Four load sensors are used to measure the normal load and friction coefficient.

Another particularity is to use an accelerometer placed at the centre of the strip to measure the vertical acceleration of the strip and estimate contact quality and the

arcing rate. The percentage of arcing is also determined by estimating the time when the contact between the wire and the strip has been lost. The contact strip temperature is obtained by means of a K-type thermocouple positioned at the centre of the contact strip [1]. Furthermore, it is possible to change the type of voltage between direct current and  $16\frac{2}{3}$  Hz or 50 Hz alternative current frequency.

## 2.2. Experimental Study of Slip Rings

In slip rings, the current, the velocity of the sliding contact, and the normal load are usually lower than the one found in the pantograph–catenary link (PCL). Similarly, there is no sweeping motion between the two entities and no external convection effect. However, three different types of test benches developed with the same methods and specialising in the study of slip rings have been found in modern literature. Table 2 summarises these test benches features.

### 2.2.1. Studies of a Sliding Electrical Contact at Low Speed

This test bench is composed of a pure copper pin in contact with a rotating electrographite disc [39] (first column in Table 2). The steady linear speed is set at  $0.5 \text{ m}\cdot\text{s}^{-1}$ , chosen with the aim of studying the impact of load and electrical current on the friction and wear behaviour. The friction coefficient is obtained thanks to a 3D piezoelectric sensor. Wear is calculated by measuring mass loss. Temperature is measured by using a K-type thermocouple, located 2 mm away from the interface between the copper and the carbon, inside the copper span. During studies, the temperature is used as an indicator more than quantitative data. Raman spectrometry is used to analyse the material evolution and the oxidation layer of the copper–graphite copper.

### 2.2.2. Tribological Testing Device

The second column of Table 2 concerns a test bench where two SEC enable a closed-loop electrical circuit [40]. The contacts are in the shape of a disc with an inner diameter of 12 mm and an outer diameter of 19.5 mm. Real-time measurements of the normal load and the friction torque for each sliding contact help calculate the friction coefficient. Multi-component sensors are used to measure torque and force. A stationary sample is attached on these multi-component sensors, electrically and thermally isolated from the sensor. The current is given in current density and total current which helps see the current impact from two points of view and to know the contact area. Wear is determined using the sliding distance, the normal load, and the mass loss measured before and after the test. To validate the repeatability of the data, each test was performed three or four times. Three different carbonaceous materials with known properties are used and studied.

### 2.2.3. Slip Ring Brush Tribostester

(In Table 2, see the third column for the experimental setup used by Shin W.-G. and Lee S.-H. [41], the fourth column for the one used by Turel A. et al. [42], and the fifth column for a test bench used by Zhao H. [43]). Two brush samples are under pressure with a rotating disc. An electrical current flows through one brush and exits at the opposite brush. Springs are used to set a constant pressure between brush samples and commutator.

In a study by Shin W.-G. and Lee S.-H. [41] (Figure 5), contact temperature is measured by means of two T-type thermocouples installed within 3 mm from the contact. Measurements are carried out on the anode(+) and the cathode(-), leading to different results.

In the tests by Turel A. et al. [42], the test bench is introduced in an isolated chamber to control ambient temperature. From this temperature chamber, two openings are connected to a chamber in which a heater has been placed. Using K-type thermocouples helps set the ambient temperature from  $22 \text{ }^\circ\text{C}$  to  $200 \text{ }^\circ\text{C}$  with a  $\pm 2 \text{ }^\circ\text{C}$  tolerance. Additionally, relative humidity is measured.

Zhao H. has led experiments to investigate the potential use of  $\text{Cu-Ti}_3\text{AlC}_2$  sliding against a  $\text{Cu-5\%Ag}$  alloy. To characterise the samples' electrical wear performance, the main

indicators were voltage drop, friction coefficient, and wear rate. The friction coefficient is measured through a power loss approach as follows:

$$\mu = \frac{P - P_0}{N_B F_r v} \quad (3)$$

with  $\mu$  the friction coefficient [-],  $P$  the load power of the motor when the brushes make contact with the motor [W],  $P_0$  the no-load power without the brushes [W],  $N_B$  the number of brushes,  $F_r$  the contact pressure [N] and  $v$  the sliding speed [ $\text{m}\cdot\text{s}^{-1}$ ].

The wear rate is calculated with the formula:

$$W_s = \frac{\Delta M}{\rho F_r S} \quad (4)$$

with  $W_s$  the wear rate [ $\text{mm}^3\cdot(\text{N}\cdot\text{m})^{-1}$ ],  $\Delta M$  the mass loss [kg],  $\rho$  the density of the sample [ $\text{kg}\cdot\text{mm}^{-3}$ ],  $F_r$  the normal load [N] and  $S$  the sliding distance of the samples [m].

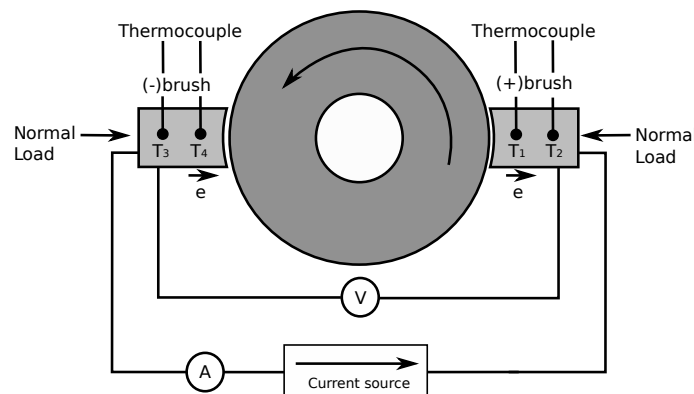


**Figure 5.** Outline of the wear test from an article by Shin W-G. and Lee S-H. [41].

### 2.3. Other Studies of Electrical Sliding Contacts

#### 2.3.1. Electrical Arc Generation

Represented by Figure 6a, a test bench allows the study of arc erosion characteristics specifically [44]. The cathode, attached under the static stage, is made of pure copper while the anode, attached on the dynamic edge, is a Cu-impregnated carbon strip material. When starting a test, the electrodes are in contact and the contact is checked ( $R_c = 10.8 \text{ m}\Omega$ ). Then, the movable stage moves at a speed of  $1 \text{ mm}\cdot\text{s}^{-1}$ . The electric arc occurs when a rupture of the contact appears while the anode is moving. The lack of representativeness has been admitted by the author. Indeed, the electric arc is elongated with the motion of the strip in a real pantograph–catenary system [45,46], whereas the arc remains stuck to its roots during tests. The arc exists in a particular region of the strip and remains stuck to its roots. During the test, the temperature distribution is recorded with an infrared camera, and the voltage waveform by a digital oscilloscope. This allows for following the arc position and its process.

#### **Triboelectrical test bench of a vibrating sliding contact**

As shown in Figure 6.b, two horizontal crossed cylinders are used to investigate a sliding electrical contact. A spring applies a 10 N normal load between the cylinders [6]. An electrical current of 5 A flows through the electrodes, with the upper electrode as the cathode and the lower as the anode. Those electrodes are 20 mm high and 10 mm in diameter. A vibrator moves the lower electrode at a 5 mm amplitude and with 3 Hz frequency. The four-point probes method is used to measure voltage drop and current. These values allow for calculating the contact resistance more accurately without taking into account contributions by wires and other contact points. Contact resistance is then observed during a test. In an article by Grandin M., three different carbon-impregnated Cu are studied and mounted on the moving part (anode), whereas the stationary part (cathode)

is made of copper. These tests are repeated for reproducibility regarding the specific wear rates and the friction coefficient.

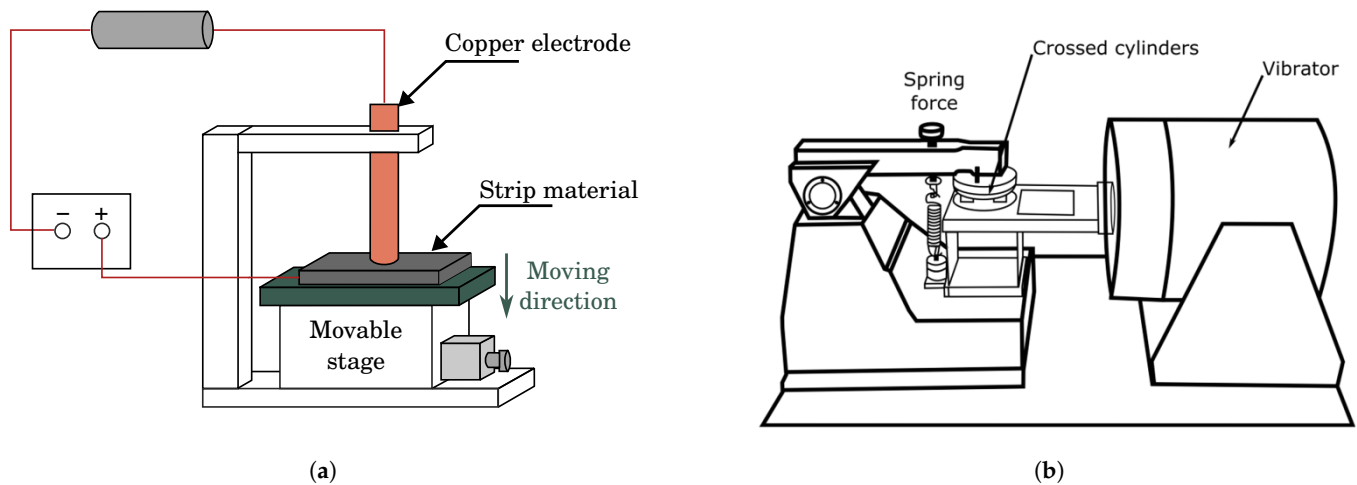


**Figure 6.** (a) Outline from an article by Wu G. et al. [44] of arc generator. (b) Outline of the experimental setup from an article by Granding M. [6]. Copyright (2023), with permission from Elsevier.

#### 2.4. Conclusions

Test benches aim to study different parameters and characteristics composing a sliding electrical contact. However, every test bench is built differently, and their respective sliding electrical contacts are not fully representative. Several parameters such as vibrations, materials, or mechanical structure can lead to different results when carried out on two test benches. Besides, the physical properties of materials regarding tree directions are not defined. The real contact area is an important feature that impacts the contact pressure, the current density, the contact resistance, wear, and the friction coefficient. Furthermore, the materials used are often different. Therefore, the experimental results of different studies will be synthesised in the next section. We will focus on the impacts of the different inputs on wear.

### 3. Discussion

This discussion is a comparison of the different experimental results obtained by scholars. As the test bench and test conditions are all different, the trends of the outputs (friction coefficient, temperature, wear) are listed depending on five major inputs: the environment, the material, the normal load, the sliding speed, and the current.

#### 3.1. Environmental Influences

Few studies have been conducted to explore the impact of the environment. Authors have focused on two environmental properties: ambient temperature and air composition.

##### 3.1.1. Ambient Temperature

An experiment led by Liu X. et al. [47] show that the friction coefficient and wear rate are higher at 100 °C than at room temperature: the high temperature increases the graphite plasticity and catalyses copper oxidation formation. Therefore a material with high copper content is more sensitive to ambient temperature changes due to its sensitivity to oxidation. Furthermore, the friction film can be destroyed more easily at high temperatures resulting in oxidative wear.

Liu R. et al. [48] performed experiments when the room temperature was controlled. They observed that the oxygen content of the materials' surface increases at high temperatures. This highlights the catalysis effect of temperature on the oxidation mentioned above. They also measured that the wear rate increases with the ambient temperature.

### 3.1.2. Gaseous Environment

Experiments made by Hu Z.L. et al. [7] have shown that the wear rate of electrographite brushes is more than twice as high at 10% relative humidity (RH) than at 50%. Observations show that at low RH, only graphite grains can be found at the surface whereas a cuprous oxide protective layer forms at higher RH. Indeed, the formation of this layer is facilitated by the presence of water vapour, which acts as a catalyst. Furthermore, the current allows the dissociation of water into  $H^+$  and  $OH^-$  ions, increasing the formation of  $Cu_2O$  from  $O_2$  and Cu.

Qian G. et al. [49] reached the same kind of conclusion by performing tests in a normal laboratory atmosphere and under a vacuum. The wear volume loss during tests is five times higher in vacuum conditions than in air. For the same reasons mentioned above, no oxide layer forms at the surface of the material, increasing the wear rate and the friction coefficient. At the end of the tests, the authors measured the roughness of the worn surfaces: it is more than twice as rough in vacuum conditions. This highlights the high adhesion and intensive abrasion that occurs in the absence of both water or oxygen [50].

### 3.2. Strip/Brush Material

Due to the various manufacturing processes and chemical compositions, there is a wide panel of materials used to manufacture brushes and strips. The number of scientific works on this subject has recently increased by 30% in the past two years [51]. In this study, we will focus on the sintered temperature and the metal impregnation.

#### 3.2.1. Sintered Temperature

Liu R. et al. [48] compared two resin-bonded copper–graphite brushes sintered at 910 °C and 450 °C (see Table 3). The authors observed that the high sintered temperature improves the bonding strength between copper and graphite. During the process, high amounts of gases are emitted at high temperatures, leading to an increase in porosity [52]. Experimental results have shown that material sintered at high temperatures has better abrasion resistance and therefore better wear performance at ambient temperatures. However, due to its higher porosity, its resistance to oxidative wear is poor, leading to lower wear performance at a higher ambient temperature than for material sintered at 450 °C.

**Table 3.** Main characteristics of materials used by cited authors.

Process	Sintered Temperature [°C]	Metal [%]	Misc [%]	Hardness [HR10-392]	Resistivity [ $\mu\Omega$ .mm]	Opening Porosity	Flexual Strength [Mpa]
Dry powder mixed Compressed (150 Mpa) Sintered 6 h	450	62	1.5 Sn	64.3	901	8	23.8
	910		4 MoS2 4.5 Resin	45.6	785	17.5	32.4

#### 3.2.2. Copper Impregnation

Copper is mainly used to impregnate carbon and the three studies presented in this section employ this metal [6,31,47]. Due to the higher electrical conductivity of copper, the electrical resistance of the material drops sharply with the increase in copper amount in the material [53]. It has also been observed that contact resistance decreases with the amount of impregnated copper [6,31].

Figure 7a represents the wear rate measured during tests depending on copper impregnation amount. From these measures and the authors' arguments, Figure 7b explains the dependence of the wear with the copper content of the material: (1) Without copper and only graphite, the electrical contact resistance is high, thus increasing the heat at contact point [47]. (2) The effect of a small amount of copper is less clear: from 0% to 50% copper content, Liu X. et al. [47] observed an increase in wear rate due to the weakening of the

structure material and the low bonding strength between copper and graphite. On the other hand, Grandin M. et al. [6] observed a decrease in the wear rate when the copper content ranges from 6 to 26%. (3) A copper matrix starts to form with higher copper content. This strengthens the materials and decreases wear rate, till reaching an optimum point (4) when wear rate is at the minimum. (5) When reaching a very high copper content, the graphite quantity spread on the surface is insufficient. Then, the contact loses the self-lubrication properties related to graphite and the protective film of  $\text{CuO}_2$  and graphite tends to wear. Therefore the roughness of the surface increases and leads to a loss in current-carrying efficiency and stability. Furthermore, high content of copper leads to greater weakness to oxidative wear [47]. Results by Yang Z. et al. [31] confirm these trends and show that the wear rate increases with high copper contents. (6) Finally, concerning a copper material with no graphite, the wear rate is high because of poor lubrication of the contact. As shown by Yang Z. et al. [31], a high coefficient friction is measured and the surface is rough, creating an unstable contact with a low current-carrying efficiency and stability.

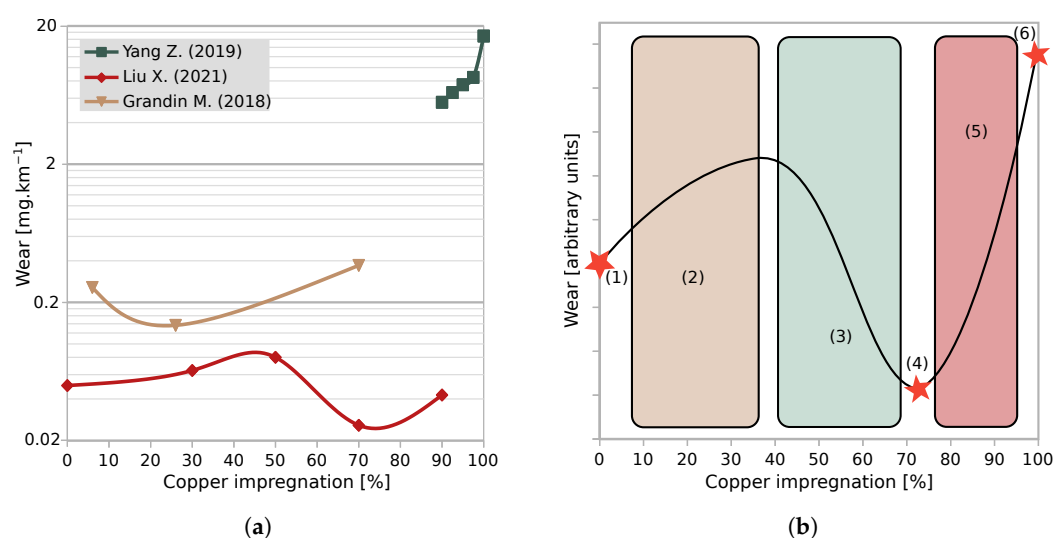


**Figure 7.** (a) Wear measures depending on copper impregnation in graphite material from three authors [6,31,47]. (b) Typical dependence of wear depending on the copper content in graphite: (1) full graphite material has a high contact electrical resistance; (2) low copper content weakens the material structure; (3) formation of a copper matrix that strengthens the material; (4) optimal point; (5) high copper content weakens the material due to oxidation sensitivity; (6) without the self-lubrication of the graphite, the wear of full copper material is high.

We have shown that the copper impregnation content has a direct influence on the wear rate of the material. The authors found that, at an optimum point, the wear rate is minimum at a specific copper content. However, some points should be highlighted:

- As for the optimal point, the amount of copper is different from one author to the other.
- The effects on the friction coefficient and the wear rate of the copper oxide  $\text{Cu}_2\text{O}$  found on the surface are still unclear.
- Authors did not observe the same wear rate trend at low amounts of copper content.

### 3.3. Normal Load

#### 3.3.1. Impact of Normal Load on Mechanical Wear Versus Electrical Wear

Undoubtedly, increasing the normal load without any current increases the abrasive wear of the strip and the contact temperature by friction heat. Indeed, Holm R. [54] expressed the mass loss  $\Delta m$  [ $\text{mg.s}^{-1}$ ] from mechanical wear with the following equation:

$$\Delta m = kpAv \quad (5)$$

where  $k$  is the wear factor [ $\text{s}^2 \cdot \text{m}^{-4}$ ],  $p$  is the normal load [N],  $A$  is the apparent contact area [ $\text{m}^2$ ], and  $v$  is the sliding velocity [ $\text{m} \cdot \text{s}^{-1}$ ].

Therefore, the normal load should be expressed accompanied by the apparent contact area and the geometry of the contact to get the normal load, which is not the case for most articles.

Regarding electrified contacts, most results show that increasing the normal load between materials decreases the wear rate [34,41,55–58], the contact heating [34,35,41,57], and the friction coefficient [40,41,56]. First, this is due to the power loss into the contact point due to Joule effect:

$$P_c = IU_c = R_c I^2 \quad (6)$$

where  $P_c$  is the power loss [W],  $R_c$  the contact resistance [ $\Omega$ ],  $U_c$  the contact voltage [V], and  $I$  the current [A].

Increasing the normal load between asperities results in an increase in contact spots [26]. Thus, the electrical contact resistance decreases due to a larger real contact area. Wang W. [59] observed this trend by calculating the power loss and measuring the contact resistance when changing the normal load.

Secondly, increasing the normal load tends to decrease the arcing rate [38] and the arc discharge energy [34,35] leading to a decrease in the wear by arcing. This influence is explained by the decrease in the contact loss rate between the strip and the contact wire.

Braunovic M. [60] describes the wear of brushes in an electric sliding contact as a function of the normal load with a U-type curve (see Figure 8a). First, the total wear drops rapidly with a decrease in electrical wear. After the optimum point, the total wear rises as the mechanical wear increases. This optimum point depends on various types of electrical machines. This behaviour is also described by Poljanec D. et al. [40] with three different materials (hard carbon, electrographite, and polymer bonded graphite) and by Wang Y.A. et al. [61]. However, Zhao H. et al. [62] had contradictory experimental results (see Figure 8b) but they did not comment on the reverse U shape of the curve. Yet, they mentioned that there is an optimum point.

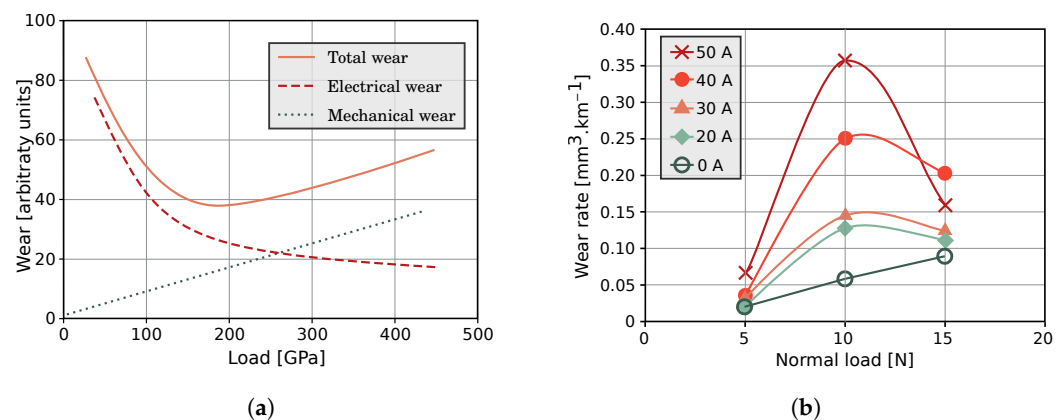


**Figure 8.** (a) Typical dependence of wear of electric machine brushes on load, from a book by Braunovic M. [60]. (b) Effect of load on the wear rate of the pin, from an article by Zhao H. et al. [62].

### 3.3.2. Parameters Related to the Normal Load

- Periodic fluctuations:** It is known that the contact force fluctuates due to the geometry of the catenary [63,64]. Zhang Y. et al. [29] observed that a periodic fluctuation of the normal load also influences the current carrying stability, its efficiency, and the arcing rate. In this work, the normal load is modulated in frequency  $f$  and amplitude  $B$  and the results obtained have shown that the arcing rate increases when  $f$  and  $B$  increase [18]. Model, force fluctuation, span length, preload, and speed. Strip spacing, friction coefficient, and lift force. More spacing between strips, more lift force, and friction coefficient.

- **The stiffness of the contact:** A pantograph is a lumped-mass system of three levels. The value of the stiffness and the lump have a direct impact on the contact behaviour and the behaviour of the contact force [63,64]. Stiffness has been experimentally studied by Ding T. et al. [65]. They observed that stiffness has a significant effect on the friction coefficient and the wear rate. The latter increases at the extreme stiffness values: slightly with low stiffness and sharply when stiffness becomes too high, reaching a maximum when the contact is strongly rigid. These variations are explained by vibration, which leads to arc discharge. The impact of stiffness is different depending on the sliding speed and the current. Nonetheless, it has been found that an optimal stiffness value leads to wear minimisation.
- **Contact area:** By setting an inclination angle between the contact strip and the wire, Chen G. et al. [34] changed the contact area and thus the contact pressure between the strip and the wire. The increase in the contact pressure results in decreasing the friction coefficient and the temperature of the contact. It also reduces the wear rate and the scaled accumulated energy (see Equation (2)), especially at low normal load (30 N).

### 3.4. Sliding Speed

The impact of the sliding speed on the behaviour of a sliding electrical contact depends on the studied system and it is necessary to differentiate between the pantograph–catenary link (PCL) and a slip ring system. Indeed, speed ranges are different (3 to 15 m.s<sup>-1</sup> in a slip ring system and 13 to 100 m.s<sup>-1</sup> in a PCL), mechanical vibrations differ from one system to another, and the convection is much higher in the PCL.

#### 3.4.1. Slip Ring

In this system, the sliding speed without current increases the wear rate of the brush and its temperature due to mechanical friction [41,62]. With current, the sliding speed decreases the wear rate, the friction coefficient, and the electrical resistance [41,42]. No hypothesis has been suggested to explain this observation. Poljanec D. et al. [40] highlighted an exception with electrographite: the wear rate increases with high values of sliding speeds (10 m.s<sup>-1</sup>), even with electrical current. This can be due to contact instabilities owed/due to surface film discontinuity on the friction track. Turel A. et al. [42] observed that applying a low sliding speed increases the wear rate at low current densities and high ambient temperatures.

#### 3.4.2. Pantograph–Catenary Link

Phenomena observed in the pantograph–catenary experiments are different. An increase in arc [36,38] and in arc-discharge energy [35] has been highlighted when the sliding speed increases. This causes temperature to increase [35] and wear rate to rise [35,38,58,66]. In the study by Zhang Y. et al. [29], mentioned in the previous section, the arcing rate has been observed to rise with the sliding speed. The effect of the sliding speed is greater when the normal load fluctuates. This trend is mainly due to an increase in vibrations and contact losses.

In PCL, Derosa S. et al. [10] have studied the impact of the sliding speed on the CCTB. They have shown that a slow sliding speed leads to the accumulation of heat and therefore to significant wear. A threshold speed of 330 mm.s<sup>-1</sup> has been estimated, below which the strip wear variation significantly increases.

Moreover, convection must be taken into account for the PCL, since it leads the system to cool off. By doing so, Ding T. et al. [9] have shown that the wear rate of the strip decreases slightly with temperature. All the other experiments do not seem to have cooled the system in real convection conditions.

### 3.5. Current

It has been observed that the current leads to increased contact temperature [9,34,35,39–41,56,67], the friction coefficient [39,55,61,68], and the wear rate [39,42]. Its effects can be summed up in three points:

1. **The oxidation catalysis** of the contact surface impacts the friction coefficient, the wear rate, and the contact temperature;
2. **The Joule effect** produces heat due to high electrical contact resistance;
3. **Sparks and arcs discharge** when contact loss occurs, increasing the temperature and wear rate.

#### 3.5.1. Catalysis Oxidation

When the current is set, the friction coefficient drops at once [56,69]. Indeed, the current acts as a catalyst for oxidation reactions in two ways [7,70,71]. First axis: the current brings electrons that accelerate the oxidation process. Second axis: the heat produced by the Joule effect and electrical arcs readily cause oxidation (see Section 3.1).

By heating the sample, Ding T. et al. [9] measured that the heat itself, rather than the current, decreases the friction coefficient (see Figure 9).

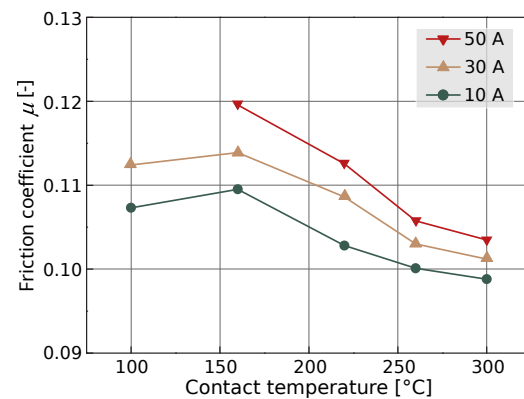


**Figure 9.** Current and temperature effects on the friction coefficient from an article by Ding T. et al. [9].

#### 3.5.2. Heat by Joule Effect

The power dissipated by Joule effect is given by Equation (6). As the current increases, and without vibration, the Joule effect quickly becomes the main heat source. When heat is too high, the material can soften locally, so that it more easily generates wear debris, flake-like delamination, and ploughing [9].

#### 3.5.3. Arcing

Arcing happens in case of contact instabilities in which contact stiffness [65], normal loading [34,39,41,56], and sliding velocity [29,35,36,38,72] play a key role. Here are the chronological steps of the impact of arcs discharge:

1. The very high temperature can melt or turn materials into gas [73]: the melted impregnated copper (1357 K) can yield copper ionisation that accelerates the oxidation processes. Furthermore, copper can gasify (2848 K), and so can as well as the carbon (4073 K) [44];
2. Melted copper asperities can solidify directly close to the contact. The resulting particle makes grooves and ridges on the friction track due to the tangential force, making the surface rougher. This also enhances abrasive wear rate [74];
3. The exudate copper from impregnated carbon can form a metallic film [74];
4. After arcing, some cracks can be observed on the surface. This could be due to the non-homogenous thermal conduction properties of the material, leading to thermal strain between the carbon substrate and the impregnated copper. Crack nucleation can then occur through contact fatigue [74].

#### 3.5.4. Direction of Current Flow

The flow direction of the current impacts the contact behaviour. In a copper–graphite sliding contact, Senouci A. [75] and other authors [76–78] observed that the friction coefficient and the contact resistance are not the same depending on the directions of the current. The contact resistance doubles when copper is the cathode and graphite the anode, whereas the friction coefficient decreases slightly. In this case, the third body is a mixture of carbon–copper oxides. Indeed, the current inhibits the growth of the copper oxides and metallic bonds are created between copper and graphite. However, when copper constitutes the anode, the third body is made of a thin copper oxide layer, which has a great impact on the contact behaviour [79]. Carbon’s higher electrical resistance and self-lubricant properties explain these behaviours. Shin W.G. et al. [41] and Bares J.A. et al. [2] observed the same results.

In PCL, Midya.S et al. [45,46] observed that the arc’s root tends to maintain more easily when the strip is the cathode, due to slow sliding speed. On the contrary, when the wire is the cathode, the arc tends to break more easily, leading to more frequent open contact. Authors indicate that the root of the cathode needs more energy to move than that of the anode.

#### 3.5.5. Wear Rate

Multiple correlations have been highlighted between the temperature or arc discharge and the wear rate. From Figure 10a, Chen G.X. [35] observed that the wear rate is clearly linearly correlated with contact temperature. On the same test bench, Mei G. also made a linear correlation between arc discharge and wear rates (see Figure 10b), but also between the contact temperature and the arc discharge energy rate [80]. This shows that the accumulated heat is directly related to electrical arcs. Finally, by heating the sample at different temperatures, Ding T. [9] measured wear volume with and without current. Figure 10c highlights that the wear volume increases with the current, almost linearly. This last trend is also confirmed by Kubo.S and Kato.K [81] and Kubota.Y [68]. A contact at room temperature, or cooled, leads to a slightly positive impact on the mass loss of the strip, but the wear rate is mainly very much dependent on the current. The wear rate is therefore the combination of arcing and temperature increase from the Joule effect. Therefore, the fast arc discharge becomes the main reason for a high wear rate [38,82].

Figure 11 gives an overview of the wear process caused by the current. As discussed above, the latter has three effects, with a direct or indirect impact on the wear rate. Firstly, it is known that arc discharge has a direct and negative impact. Secondly, with the heat from the Joule effect and electron flow, the current is a catalyst for oxidation. This can be negative or positive for wear since the oxidation modifies the tribofilm properties and the friction coefficient [83]. However, although the impact is not straightforward, the current always increases the wear rate of the material [9,38,82,84,85].

- When increasing the normal load, a downward trend of the wear rate is most often observed. Nevertheless, this trend is controversial among scholars. Furthermore, the stiffness of the strip plays a key role in vibration and arc occurrence, yet it has been discussed very little.
- The causes of wear are also being discussed and processes are still not well understood when the current is flowing. Electric arc and Joule effects are the main factors in the wear of electric sliding contact. Yet, from a chemical standpoint, the role of current flowing through copper and graphite has not been much studied.
- Through the articles mentioned and their results, specific wear rate and wear rate are both used to quantify wear properties. Results show strong differences from one another.
- The material used as a strip of course plays a key role in the wear mechanism and the behaviour of the electrical sliding contact. As a matter of fact, the manufacturing process, impregnated rate, impregnated process, hardness, and electrical resistance have been said to change the wear rate, the friction coefficient, and contact temperature

increase. Materials also have displayed different behaviours when changing the normal load, the sliding speed, and the current flow.

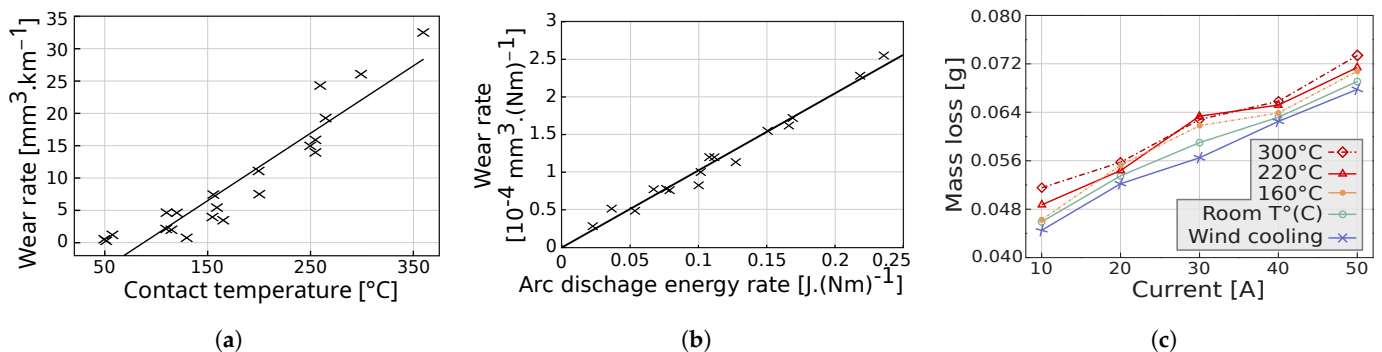


**Figure 10.** (a) Correlation between the temperature of the contact strip and the wear rate from an article by Chen G.X. [35]. (b) Correlation between the arc discharge energy rate and the wear rate, from an article by Mei G. [80]. (c) Mass loss of the carbon strip according to the variation of the current at different temperatures, from an article by Ding T. et al. [9].

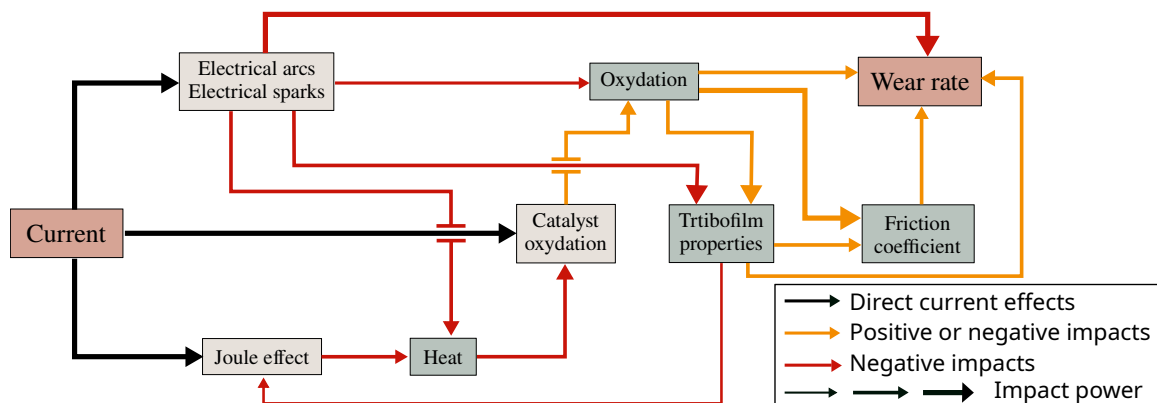


**Figure 11.** Impacts of the current on the wear of materials found in sliding electrical contacts.

#### 4. Conclusions

In this study, numerous test benches presented have helped synthesise the behaviour of a SEC. Most of them are in some way representative of the slip ring system or the pantograph–catenary link. They also have their own specificities and field of study. Owing to the different geometries and structures, as well as the type of measurements, (intrusive vs. non-intrusive), experimental results cannot be directly compared. Therefore, following these results, mainly trends have been highlighted. The impacts of the major entries of a SEC—that is the environment, the material, the normal load, the sliding speed and the current—have been explained that way.

Figure 12 shows an overview of the discussed experimental results. Some sections, such as the current effects or the environmental influence, can be clearly synthesised. As a matter of fact, multiple authors suggest the same trends and explanations, which strengthen the synthesis. However, the behaviour obtained with different materials and at different contact forces or sliding speeds cannot be clarified so readily. Either some results are contradictory, like the trends of the wear measured at different normal load or at different speeds, or research is lacking and published works are insufficient.

##### Material

For studies concerning copper impregnation of graphitic materials, the results obtained are similar, but their study boundary and result dispersion weaken these remarks. The significance of the sintered temperature of the material is easily explained away but based on a single reference. Furthermore, other process characteristics like pressure, time of mixing, or type of impregnation could be studied. Furthermore, few authors mention

the full composition of the material used in their work. Finally, the direction of material could be studied to have a better understanding of the anisotropic behaviour of graphite.

#### Contact force

Most papers indicate that the wear found in SEC follows the trend described by Braunovic M. [60]. However, some results are contradictory, and by specifying the stiffness and measuring the vibrations during experiments, one could have a better understanding of the phenomena involved. Furthermore, an approximation and a study of the significance of the contact area could be very interesting.

#### Sliding speed

In the pantograph–catenary link, the impact of the convection on the contact could be more investigated, as it is not taken into account in most studies. The deflection and aerodynamics could also be interesting to experimentally study. In slip ring systems, the results of different papers are contradictory and it is not possible to clearly state whether sliding speed affects the wear rate and the heat of the brush. Therefore, more investigations are needed to clarify this point.

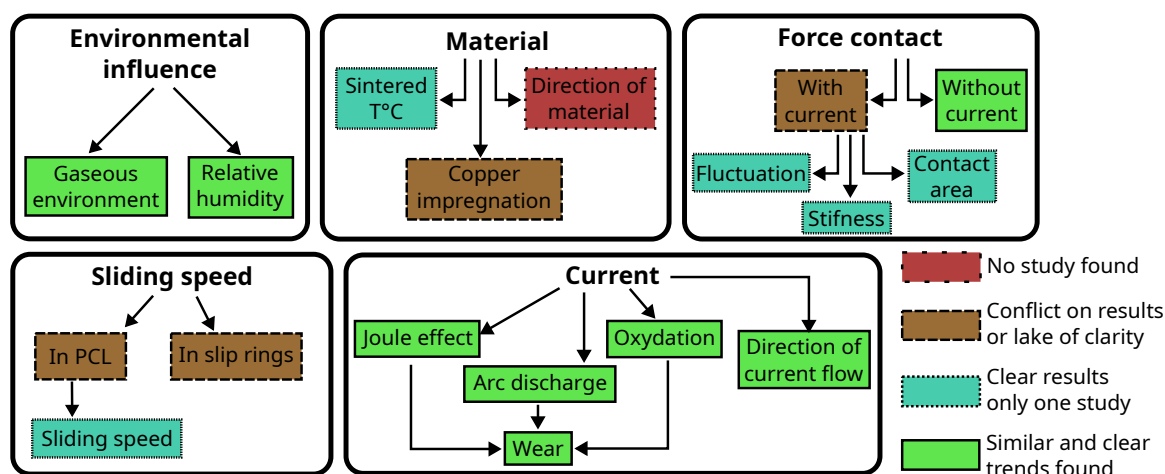


**Figure 12.** Overview of the numerous fields of study focusing on sliding electrical contacts, their progress, and lack of studies.

From the different entries of an SEC, the current doubtlessly most impacts the behaviour of the contact temperature, the friction coefficient, or the wear rate. It is also the entry whose effects are best known and explained. However, the interaction of the current with the sliding speed, the normal load, or the geometry of the contact should be explored.

**Author Contributions:** Writing—original draft preparation, T.K.; writing—review and editing, T.K., E.G., P.B., P.-H.C. and D.C.; validation, E.G., P.B., P.-H.C. and D.C.; supervision, E.G., P.B. and D.C.; All authors have read and agreed to the published version of the manuscript.

**Funding:** This research received no external funding.

**Acknowledgments:** This work has been supported by EIPHI Graduate School, contract <ANR-17-EURE-0002>.

**Conflicts of Interest:** The authors declare no conflict of interest.

#### Abbreviations

The following abbreviations are used in this manuscript:

SEC	Sliding electrical contacts
SEM	Scanning electron microscopy
EDS	Energy dispersive spectroscopy
CCTB	Current collection test bench
PCL	Pantograph–catenary link

## References

1. Delcey, N.; Baucour, P.; Chamagne, D.; Wimmer, G.; Bucca, G.; Bruyere, N.; Bouger, O.; Auditeau, G.; Bausseron, T. Analysis of the thermal variations in a moving pantograph strip using an electro-thermal simulation tool and validating by experimental tests. *Proc. Inst. Mech. Eng. Part F J. Rail Rapid Transit* **2019**, *234*. <https://doi.org/10.1177/0954409719877341>.
2. Bares, J.; Argibay, N.; Mauntler, N.; Dudder, G.; Perry, S.; Bourne, G.; Sawyer, W. High current density copper-on-copper sliding electrical contacts at low sliding velocities. *Wear* **2009**, *267*, 417–424. <https://doi.org/10.1016/j.wear.2008.12.062>.
3. He, D.H.; Manory, R. A novel electrical contact material with improved self-lubrication for railway current collectors. *Wear* **2001**, *249*, 626–636. [https://doi.org/10.1016/s0043-1648\(01\)00700-1](https://doi.org/10.1016/s0043-1648(01)00700-1).
4. Ordoñez, M.; Farias, M.; Descartes, S.; Machado, I.; Souza, R. Tribofilm formation during dry sliding of graphite- and MoS<sub>2</sub>-based composites obtained by spark plasma sintering. *Tribol. Int.* **2021**, *160*, 107035. <https://doi.org/10.1016/j.triboint.2021.107035>.
5. Bausseron, T.; Baucour, P.; Glises, R.; Verschelde, S.; Chamagne, D. Experimental study and modelling of overheating of electrical catenary-pantograph interface for trains supplied with power in station. *Eur. Phys. J. Appl. Phys.* **2015**, *70*, 30901. <https://doi.org/10.1051/epjap/2015140262>.
6. Grandin, M.; Wiklund, U. Wear phenomena and tribofilm formation of copper/copper-graphite sliding electrical contact materials. *Wear* **2018**, *398–399*, 227–235. <https://doi.org/10.1016/j.wear.2017.12.012>.
7. Hu, Z.; Chen, Z.; Xia, J. Study on surface film in the wear of electrographite brushes against copper commutators for variable current and humidity. *Wear* **2008**, *264*, 11–17. <https://doi.org/10.1016/j.wear.2007.01.034>.
8. Zhang, Y.; Li, C.; Pang, X.; Song, C.; Ni, F.; Zhang, Y. Evolution processes of the tribological properties in pantograph/catenary system affected by dynamic contact force during current-carrying sliding. *Wear* **2021**, *477*, 203809. <https://doi.org/10.1016/j.wear.2021.203809>.
9. Ding, T.; Chen, G.; Bu, J.; Zhang, W. Effect of temperature and arc discharge on friction and wear behaviours of carbon strip/copper contact wire in pantograph—catenary systems. *Wear* **2011**, *271*, 1629–1636. <https://doi.org/10.1016/j.wear.2010.12.031>.
10. Derosa, S.; Nàvik, P.; Collina, A.; Bucca, G.; Rønquist, A. Contact point lateral speed effects on contact strip wear in pantograph — catenary interaction for railway operations under 15 kV 16.67 Hz AC systems. *Wear* **2021**, *486–487*, 204103. <https://doi.org/10.1016/j.wear.2021.204103>.
11. Bucca, G.; Collina, A. Electromechanical interaction between carbon-based pantograph strip and copper contact wire: A heuristic wear model. *Tribol. Int.* **2015**, *92*, 47–56. <https://doi.org/10.1016/j.triboint.2015.05.019>.
12. Mei, G.; Song, Y. Effect of Overhead Contact Line Pre-Sag on the Interaction Performance with a Pantograph in Electrified Railways. *Energies* **2022**, *15*, 6875. <https://doi.org/10.3390/en15196875>.
13. Song, Y.; Zhang, M.; Øiseth, O.; Rønquist, A. Wind deflection analysis of railway catenary under crosswind based on nonlinear finite element model and wind tunnel test. *Mech. Mach. Theory* **2022**, *168*, 104608. <https://doi.org/10.1016/j.mechmachtheory.2021.104608>.
14. Materra, J.P. Développement d'un outil de modélisation électrothermique d'une caténaire du domaine ferroviaire. Ph.D. Thesis, Université de Franche-Comte, Besançon, France, 2010.
15. Song, Y.; Liu, Z.; Wang, H.; Lu, X.; Zhang, J. Nonlinear analysis of wind-induced vibration of high-speed railway catenary and its influence on pantograph–catenary interaction. *Veh. Syst. Dyn.* **2016**, *54*, 723–747. <https://doi.org/10.1080/00423114.2016.1156134>.
16. Song, Y.; Liu, Z.; Rønquist, A.; Navik, P.; Liu, Z. Contact Wire Irregularity Stochastics and Effect on High-speed Railway Pantograph-Catenary Interactions. *IEEE Trans. Instrum. Meas.* **2020**, *69*, 8196–8206. <https://doi.org/10.1109/tim.2020.2987457>.
17. Song, Y.; Antunes, P.; Pombo, J.; Liu, Z. A methodology to study high-speed pantograph-catenary interaction with realistic contact wire irregularities. *Mech. Mach. Theory* **2020**, *152*, 103940. <https://doi.org/10.1016/j.mechmachtheory.2020.103940>.
18. Simarro, M.; Castillo, J.J.; Cabrera, J.A.; Postigo, S. Evaluation of the influence of the speed, preload and span length on the contact forces in the interaction between the pantograph and the overhead conductor rail. *Eng. Struct.* **2021**, *243*, 112678. <https://doi.org/10.1016/j.engstruct.2021.112678>.
19. Pappalardo, C.M.; Patel, M.D.; Tinsley, B.; Shabana, A.A. Contact force control in multibody pantograph/catenary systems. *Proc. Inst. Mech. Eng. Part K: J. Multi-Body Dyn.* **2016**, *230*, 307–328. <https://doi.org/10.1177/1464419315604756>.
20. Daocharoenporn, S.; Mongkolwongrojn, M.; Kulkarni, S.; Shabana, A.A. Prediction of the Pantograph/Catenary Wear Using Nonlinear Multibody System Dynamic Algorithms. *J. Tribol.* **2019**, *141*. <https://doi.org/10.1115/1.4042658>.
21. Jia, S.; Liu, P.; Ren, F.; Tian, B.; Zheng, M.; Zhou, G. Wear behavior of Cu—Ag—Cr alloy wire under electrical sliding. *Mater. Sci. Eng. A* **2005**, *398*, 262–267. <https://doi.org/10.1016/j.msea.2005.03.023>.
22. Dai, Z.; Li, T.; Deng, J.; Zhou, N.; Zhang, W. Effect of the strip spacing on the aerodynamic performance of a high-speed double-strip pantograph. *Veh. Syst. Dyn.* **2021**, *60*, 3358–3374. <https://doi.org/10.1080/00423114.2021.1945117>.
23. Dai, Z.; Li, T.; Zhou, N.; Zhang, J.; Zhang, W. Numerical simulation and optimization of aerodynamic uplift force of a high-speed pantograph. *Railw. Eng. Sci.* **2022**, *30*, 117–128. <https://doi.org/10.1007/s40534-021-00258-7>.
24. Carnevale, M.; Facchinetti, A.; Maggiori, L.; Rocchi, D. Computational fluid dynamics as a means of assessing the influence of aerodynamic forces on the mean contact force acting on a pantograph. *Proc. Inst. Mech. Eng. Part F J. Rail Rapid Transit* **2016**, *230*, 1698–1713. <https://doi.org/10.1177/0954409715606748>.

25. Yang, Z.; Xu, P.; Wei, W.; Gao, G.; Zhou, N.; Wu, G. Influence of the Crosswind on the Pantograph Arcing Dynamics. *IEEE Trans. Plasma Sci.* **2020**, *48*, 2822–2830. <https://doi.org/10.1109/tps.2020.3010553>.
26. Derosa, S.; Nāvīk, P.; Collina, A.; Bucca, G.; Rønquist, A. A heuristic wear model for the contact strip and contact wire in pantograph—Catenary interaction for railway operations under 15 kV 16.67 Hz AC systems. *Wear* **2020**, *456–457*, 203401. <https://doi.org/10.1016/j.wear.2020.203401>.
27. Bucca, G.; Collina, A. A procedure for the wear prediction of collector strip and contact wire in pantograph—catenary system. *Wear* **2009**, *266*, 46–59. <https://doi.org/10.1016/j.wear.2008.05.006>.
28. Lin, Y.; Wu, M.; Ju, X.; Lin, W.; Ma, D.; Jin, L. Finite Element Simulation Study on Wear under Pantograph-Catenary System with Electric Current. In Proceedings of the 2020 IEEE International Conference on High Voltage Engineering and Application (ICHVE), Beijing, China, 6–10 September 2020. <https://doi.org/10.1109/ichve49031.2020.9279672>.
29. Zhang, Y.; Zhang, Y.; Song, C. Arc Discharges of a Pure Carbon Strip Affected by Dynamic Contact Force during Current-Carrying Sliding. *Materials* **2018**, *11*, 796. <https://doi.org/10.3390/ma11050796>.
30. Yang, Z.; Zhang, Y.; Zhao, F.; Shangguan, B. Dynamic variation of arc discharge during current-carrying sliding and its effect on directional erosion. *Tribol. Int.* **2016**, *94*, 71–76. <https://doi.org/10.1016/j.triboint.2015.03.012>.
31. Yang, Z.; Ge, Y.; Zhang, X.; Shangguan, B.; Zhang, Y.; Zhang, J. Effect of Carbon Content on Friction and Wear Properties of Copper Matrix Composites at High Speed Current-Carrying. *Materials* **2019**, *12*, 2881. <https://doi.org/10.3390/ma12182881>.
32. Wu, G.; Wei, W.; Gao, G.; Wu, J.; Zhou, Y. Evolution of the electrical contact of dynamic pantograph—catenary system. *J. Mod. Transp.* **2016**, *24*, 132–138. <https://doi.org/10.1007/s40534-016-0099-1>.
33. Wu, G.; Wu, J.; Wei, W.; Zhou, Y.; Yang, Z.; Gao, G. Characteristics of the Sliding Electric Contact of Pantograph/Contact Wire Systems in Electric Railways. *Energies* **2017**, *11*, 17.
34. Chen, G.; Yang, H.; Zhang, W.; Lu, Y.; Zhang, S.; Zhou, Z. Effect of the strip inclination angle on the friction and wear behavior of contact strip against contact wire with electric current. *Proc. Inst. Mech. Eng. Part J J. Eng. Tribol.* **2013**, *227*, 1406–1417. <https://doi.org/10.1177/1350650113495825>.
35. Chen, G.X.; Hu, Y.; Dong, B.J.; Yang, H.J.; Gao, G.Q.; Wu, G.N.; Zhang, W.H.; Zhou, Z.R. Experimental study on the temperature of the contact strip in sliding electric contact. *Eng. Tribol.* **2017**, *231*, 1–8.
36. Mei, G. Tribological performance of rigid overhead lines against pantograph sliders under DC passage. *Tribol. Int.* **2020**, *151*, 106538. <https://doi.org/10.1016/j.triboint.2020.106538>.
37. Bucca, G.; Collina, A.; Manigrasso, R.; Mapelli, F.; Tarsitano, D. Analysis of electrical interferences related to the current collection quality in pantograph—catenary interaction. *J. Rail Rapid Transit* **2011**, *225*, 483–499.
38. Bucca, G.; Collina, A.; Tanzi, E. Experimental analysis of the influence of the electrical arc on the wear rate of contact strip and contact wire in a.c. system. In *Advances in Italian Mechanism Science*; Springer: Berlin/Heidelberg, Germany, 2016.
39. Benfoughal, A.; Bouchoucha, A.; Mouadji, Y. Effect of electrical current on friction and wear behavior of copper against graphite for low sliding speeds. *U.P.B. Sci. Bull. Ser. D Mech. Eng.* **2018**, *80*, 117–130.
40. Poljanec, D.; Kalin, M.; Kumar, L. Influence of contact parameters on the tribological behaviour of various graphite/graphite sliding electrical contacts. *Wear* **2018**, *406–407*, 75–83. <https://doi.org/10.1016/j.wear.2018.03.022>.
41. Shin, W.G.; Lee, S.H. An analysis of the main factors on the wear of brushes for automotive small brush-type DC motor. *J. Mech. Sci. Technol.* **2010**, *24*, 37–41. <https://doi.org/10.1007/s12206-009-1135-4>.
42. Turel, A.; Slavič, J.; Boltežar, M. Electrical contact resistance and wear of a dynamically excited metal–graphite brush. *Adv. Mech. Eng.* **2017**, *9*, 1687814017694801.
43. Zhao, H.; Feng, Y.; Zhou, Z.; Qian, G.; Zhang, J.; Huang, X.; Zhang, X. Effect of electrical current density, apparent contact pressure, and sliding velocity on the electrical sliding wear behavior of Cu—Ti<sub>3</sub>AlC<sub>2</sub> composites. *Wear* **2020**, *444–445*, 203156. <https://doi.org/10.1016/j.wear.2019.203156>.
44. Wu, G.; Zhou, Y.; Gao, G.; Wu, J.; Wei, W. Arc Erosion Characteristics of Cu-Impregnated Carbon Materials Used for Current Collection in High-Speed Railways. *IEEE Trans. Components, Packag. Manuf.* **2018**, *8*, 1014–1023.
45. Midya, S.; Bormann, D.; Larsson, A.; Schutte, T.; Thottappillil, R. Understanding pantograph arcing in electrified railways—Influence of various parameters. In Proceedings of the 2008 IEEE International Symposium on Electromagnetic Compatibility, Hamburg, Germany, 8–12 September 2008. <https://doi.org/10.1109/isemc.2008.4652112>.
46. Midya, S.; Bormann, D.; Schutte, T.; Thottappillil, R. Pantograph Arcing in Electrified Railways—Mechanism and Influence of Various Parameters—Part I: With DC Traction Power Supply. *IEEE Trans. Power Deliv.* **2009**, *24*, 1931–1939. <https://doi.org/10.1109/tpwr.2009.2021035>.
47. Liu, X.; Hu, M.; Li, Z.; Zhou, C.; Xiao, Q.; Yang, W.; Chen, D. Effect of copper contents on the current-carrying wear properties of carbon brush under different temperatures conditions. *J. Mater. Res. Technol.* **2021**, *15*, 3110–3121. <https://doi.org/10.1016/j.jmrt.2021.09.111>.
48. Liu, R.; Cheng, K.; Chen, J.; Xiong, X.; Lin, X. Friction and wear properties of high temperature and low temperature sintered copper-graphite brushes at different ambient temperatures. *J. Mater. Res. Technol.* **2020**, *9*, 7288–7296. <https://doi.org/10.1016/j.jmrt.2020.04.092>.
49. Qian, G.; Feng, Y.; Li, B.; Huang, S.; Liu, H.; Ding, K. Effect of electrical current on the tribological behavior of the Cu-WS<sub>2</sub>-G composites in air and vacuum. *Chin. J. Mech. Eng.* **2013**, *26*, 384–392.

50. Senouci, A.; Zaidi, H.; Frene, J.; Bouchoucha, A.; Paulmier, D. Damage of surfaces in sliding electrical contact copper/steel. *Appl. Surf. Sci.* **1999**, *144–145*, 287–291. [https://doi.org/10.1016/S0169-4332\(98\)00915-5](https://doi.org/10.1016/S0169-4332(98)00915-5).
51. Cantürk, S.B.; Kováčik, J. Review of Recent Development in Copper/Carbon Composites Prepared by Infiltration Technique. *Energies* **2022**, *15*, 5227. <https://doi.org/10.3390/en15145227>.
52. Cheng, K.; Liu, R.; Xiong, X.; Lin, X.; Chen, J. The Effect of Sintering Temperature on the Microstructures and Properties of Resin-Bonded Copper—Graphite Brush Materials. *Tribol. Lett.* **2019**, *67*. <https://doi.org/10.1007/s11249-019-1192-5>.
53. Maňka, A.; Heľka, A.; Ćwiek, J. The Influence of Pantograph Carbon—Metal Composite Slider Thermal Properties on the Railroad Wire Temperature. *Energies* **2021**, *14*, 7940. <https://doi.org/10.3390/en14237940>.
54. Holm, R. *Electric Contacts—Theory and Application*, 3rd ed.; Springer Berlin/Heidelberg, Germany, 1967. <https://doi.org/10.1007/978-3-662-06688-1>.
55. Chen, G.X.; Li, F.X.; Dong, L.; Zhu, M.H.; Zhou, Z.R. Friction and wear behaviour of stainless steel rubbing against copper-impregnated metallized carbon. *Tribol. Int.* **2009**, *42*, 934–939.
56. Ding, T.; Xuan, W.; He, Q.; Wu, H.; Xiong, W. Study on Friction and Wear Properties of Pantograph Strip/Copper Contact Wire for High-Speed Train. *Open Mech. Eng. J.* **2014**, *8*, 125–128. <https://doi.org/10.2174/1874155x20140501005>.
57. Delcey, N. Modélisation électro-thermique d'un pantographe pour un train en mouvement. Ph.D. Thesis, Université Bourgogne-Franche Comté, Besançon, France, 2018.
58. Mei, G. Impact of voltage on the electric sliding tribological properties of current collectors against overhead lines. *Wear* **2021**, *474–475*, 203868. <https://doi.org/10.1016/j.wear.2021.203868>.
59. Wang, W.; Dong, A.; Wu, G.; Gao, G.; Zhou, L.; Wang, B.; Cui, Y.; Liu, D.; Li, D.; Li, T. Study on Characterization of Electrical Contact Between Pantograph and Catenary. In Proceedings of the IEEE 57th Holm Conference on Electrical Contacts (Holm), Minneapolis, MN, USA, 11–14 September 2011.
60. Braunovic, M.; Myshkin, N.K.; Konchits, V.V. *Electrical Contacts*; Taylor & Francis Ltd.: Abingdon-on-Thames, UK, 2017.
61. Wang, Y.; Li, J.; Yan, Y.; Qiao, L. Effect of electrical current on tribological behavior of copper-impregnated metallized carbon against a Cu—Cr—Zr alloy. *Tribol. Int.* **2012**, *50*, 26–34. <https://doi.org/10.1016/j.triboint.2011.12.022>.
62. Zhao, H.; Barber, G.; Liu, J. Friction and wear in high speed sliding with and without electrical current. *Wear* **2001**, *249*, 409–414. [https://doi.org/10.1016/S0043-1648\(01\)00545-2](https://doi.org/10.1016/S0043-1648(01)00545-2).
63. Vo-Van, O.; Massat, J.P.; Laurent, C.; Balmes, E. Introduction of variability into pantograph—catenary dynamic simulations. *Veh. Syst. Dyn.* **2014**, *52*, 1254–1269. <https://doi.org/10.1080/00423114.2014.922199>.
64. Pombo, J.; Ambrósio, J. Influence of pantograph suspension characteristics on the contact quality with the catenary for high speed trains. *Comput. Struct.* **2012**, *110–111*, 32–42. <https://doi.org/10.1016/j.compstruc.2012.06.005>.
65. Ding, T.; Chen, G.; Zhu, M.; Zhang, W.; Zhou, Z. Influence of the spring stiffness on friction and wear behaviours of stainless steel/copper-impregnated metallized carbon couple with electrical current. *Wear* **2009**, *267*, 1080–1086. <https://doi.org/10.1016/j.wear.2008.12.098>.
66. Ratovoson, P.L. Caractérisation expérimentale d'un arc impulsif. Ph.D. Thesis, Université Toulouse III Paul Sabatier, Toulouse, France, 2015.
67. Ding, T.; Chen, G.X.; Wang, X.; Zhu, M.H.; Zhang, W.H.; Zhou, W.X. Friction and wear behavior of pure carbon strip sliding against copper contact wire under AC passage at high speeds. *Tribol. Int.* **2011**, *44*, 437–444.
68. Kubota, Y. Relationship between Wear Profile of Pantograph Contact Strip and Arc Discharge Energy Distribution. In Proceedings of the 2018 IEEE Holm Conference on Electrical Contacts, Albuquerque, NM, USA, 14–18 October 2018. <https://doi.org/10.1109/holm.2018.8611784>.
69. Csapo, E.; Zaidi, H.; Paulmier, D.; Kadiri, E.; Bouchoucha, A.; Robert, F. Influence of the electrical current on the graphite surface in an electrical sliding contact. *Surf. Coatings Technol.* **1995**, *76–77*, 421–424. [https://doi.org/10.1016/0257-8972\(95\)02626-6](https://doi.org/10.1016/0257-8972(95)02626-6).
70. Bouchoucha, A.; Chekroud, S.; Paulmier, D. Influence of the electrical sliding speed on friction and wear processes in an electrical contact copper–stainless steel. *Appl. Surf. Sci.* **2004**, *223*, 330–342. <https://doi.org/10.1016/j.apsusc.2003.09.018>.
71. Grandin, M.; Wiklund, U. Friction, wear and tribofilm formation on electrical contact materials in reciprocating sliding against silver-graphite. *Wear* **2013**, *302*, 1481–1491. <https://doi.org/10.1016/j.wear.2013.02.007>.
72. Jin, M.; Hu, M.; Li, H.; Yang, Y.; Liu, W.; Fang, Q.; Liu, S. Experimental Study on the Transient Disturbance Characteristics and Influence Factors of Pantograph—Catenary Discharge. *Energies* **2022**, *15*, 5959. <https://doi.org/10.3390/en15165959>.
73. Kubo, S.; Kato, K. Effect of arc discharge on wear rate of Cu-impregnated carbon strip in unlubricated sliding against Cu trolley under electric current. *Wear* **1997**, *216*, 172–178.
74. Kubota, Y.; Nagasaka, S.; Miyauchi, T.; Yamashita, C.; Kakishima, H. Sliding wear behavior of copper alloy impregnated C/C composites under an electrical current. *Wear* **2013**, *302*, 1492–1498. <https://doi.org/10.1016/j.wear.2012.11.029>.
75. Senouci, A.; Frene, J.; Zaidi, H. Wear mechanism in graphite–copper electrical sliding contact. *Wear* **1999**, *225*, 949–953.
76. El Mansori, M.; Paulmier, D.; Ginsztler, J.; Horvath, M. Lubrication mechanisms of a sliding contact by simultaneous action of electric current and magnetic field. *Wear* **1999**, *225–229*, 1011–1016. [https://doi.org/10.1016/S0043-1648\(99\)00070-8](https://doi.org/10.1016/S0043-1648(99)00070-8).
77. Bouchoucha, A.; Zaidi, H.; Kadiri, E.; Paulmier, D. Influence of electric fields on the tribological behaviour of electrodynamic copper/steel contacts. *Wear* **1997**, *203–204*, 434–441. [https://doi.org/10.1016/S0043-1648\(96\)07424-8](https://doi.org/10.1016/S0043-1648(96)07424-8).

78. Hounkponou, E.; Nery, H.; Paulmier, D.; Bouchoucha, A.; Zaidi, H. Tribological behaviour of graphite/graphite and graphite/copper couples in sliding electrical contact: influence on the contact electric field on the surface passivation. *Appl. Surf. Sci.* **1993**, *70–71*, 176–179. [https://doi.org/https://doi.org/10.1016/0169-4332\(93\)90422-8](https://doi.org/https://doi.org/10.1016/0169-4332(93)90422-8).
79. Chapeuil, E.; Renouf, M.; Zeng, C.; Berthier, Y. Influence of Copper/Graphite Properties on the Tribological and Electrical Behavior of Copper-Graphite Third Body Layer. *Lubricants* **2018**, *6*, 109. <https://doi.org/10.3390/lubricants6040109>.
80. Mei, G.; Fu, W.; Chen, G.; Zhang, W. Effect of high-density current on the wear of carbon sliders against Cu—Ag wires. *Wear* **2020**, *452–453*, 203275. <https://doi.org/10.1016/j.wear.2020.203275>.
81. Kubo, S.; Kato, K. Effect of arc discharge on the wear rate and wear mode transition of a copper-impregnated metallized carbon contact strip sliding against a copper disk. *Tribol. Int.* **1999**, *32*, 367–378. [https://doi.org/https://doi.org/10.1016/S0301-679X\(99\)00062-6](https://doi.org/https://doi.org/10.1016/S0301-679X(99)00062-6).
82. Wu, G.; Gao, G.; Wei, W.; Yang, Z. Friction and Wear of Pantograph and Catenary. In *The Electrical Contact of the Pantograph-Catenary System*; Springer: Singapore, 2019; pp. 71–107. [https://doi.org/10.1007/978-981-13-6589-8\\_3](https://doi.org/10.1007/978-981-13-6589-8_3).
83. Lin, X.; Liu, R.; Chen, J.; Xiong, X.; Liao, N. Study on current-carrying friction and wear properties of copper-graphite brush material reinforced by organosilicon. *J. Mater. Res. Technol.* **2021**, *12*, 365–375. <https://doi.org/10.1016/j.jmrt.2021.02.094>.
84. Yang, H.; Wang, K.; Liu, Y.; Fu, L.; Cui, X.; Jiang, G.; Hu, B. The formation of the delamination wear of the pure carbon strip and its influence on the friction and wear properties of the pantograph and catenary system. *Wear* **2020**, *454–455*, 203343. <https://doi.org/https://doi.org/10.1016/j.wear.2020.203343>.
85. Yang, H.; Li, C.; Liu, Y.; Fu, L.; Jiang, G.; Cui, X.; Hu, B.; Wang, K. Study on the delamination wear and its influence on the conductivity of the carbon contact strip in pantograph-catenary system under high-speed current-carrying condition. *Wear* **2021**, *477*, 203823. <https://doi.org/https://doi.org/10.1016/j.wear.2021.203823>.

**Disclaimer/Publisher’s Note:** The statements, opinions and data contained in all publications are solely those of the individual author(s) and contributor(s) and not of MDPI and/or the editor(s). MDPI and/or the editor(s) disclaim responsibility for any injury to people or property resulting from any ideas, methods, instructions or products referred to in the content.